Letter

Electrically controllable topological magnetism in multiferroic antiferromagnetic $PbVO_3$

Yonglong Ga,[1,2,4,*] Dongxing Yu,[1,5,*] Yong Li,[3,*] Jiawei Jiang,[2] Liming Wang,[1] Peng Li,[1] Jinghua Liang,[1] Hai Feng,[3] Youguo Shi,[3,4] and Hongxin Yang[1,2,4,6,†]

[1]*Ningbo Institute of Materials Technology and Engineering, Chinese Academy of Sciences, Ningbo 315201, China*

[2]*National Laboratory of Solid State Microstructures, School of Physics, Collaborative Innovation Center of Advanced Microstructures, Nanjing University, Nanjing 210093, China*

[3]*Beijing National Laboratory for Condensed Matter Physics and Institute of Physics, Chinese Academy of Sciences, Beijing 100190, China*

[4]*Center of Materials Science and Optoelectronics Engineering, University of Chinese Academy of Sciences, Beijing 100049, China*

[5]*Key Laboratory for Magnetism and Magnetic Materials of the Ministry of Education, Lanzhou University, Lanzhou 730000, China*

[6]*Center for Quantum Matter and Device Applications, School of Physics, Zhejiang University, Hangzhou 31008, China*

(Received 25 May 2023; accepted 9 January 2024; published 5 February 2024)

We propose to realize the nonvolatile four-state antiferromagnetic (AFM) skyrmions in multiferroic oxide system with underlying asymmetry. Subsequently, through strain-mediated magnetic phase engineering, we find that AFM skyrmions can be obtained in bulk $PbVO_3$. Moreover, we also explore possible existence of AFM skyrmions in the $SrTiO_3/PbVO_3$ ($PbTiO_3/PbVO_3$) heterostructures via *ab initio* calculations, where AFM skyrmions can still survive. Eventually, we realize four-state AFM skyrmions (**P**↑,**L**↓), (**P**↑,**L**↑), (**P**↓,**L**↓), and (**P**↓,**L**↑) with different chirality induced by polarization (**P**) switching and polarity arising from magnetization (**L**) reversal in multiferroic $PbVO_3$. In this letter, we provide an avenue toward electric-field control of AFM skyrmions in multiferroic oxides and offer perspectives for designing AFM skyrmion-based spintronic devices.

DOI: 10.1103/PhysRevB.109.L060402

Introduction. The search for intrinsic multiferroic compounds that can realize electrically switchable topological magnetism has been an intensive topic in spintronics [1–6]. Both space-inversion asymmetry and time-reversal symmetry breaking in multiferroics can induce fourfold degenerate chiral states, which can provide a pathway toward multibit memory and logic devices [7–10]. More recently, chiral spin configurations, e.g., chiral domain walls [11], magnetic skyrmions [12,13], and bimerons [14,15], which are stabilized by the Dyzaloshinskii-Moriya interaction (DMI) in noncentrosymmetric magnets with spin-orbit coupling (SOC) [16–18], are of great interest as ideal information carriers for future spintronic applications [1,19–24]. Experimental reports have revealed that topologically protected spin textures can be observed in multiple magnetic systems, such as B20 [13,25,26], ferromagnet (FM)/heavy metal (HM) thin films [27–30], Heusler compounds [31,32], and multiferroics [33,34]. Among these, multiferroic materials combining ferroelectricity and magnetism provide the opportunity to obtain four states from the perspective of symmetry [8,9,35], which enable the possibility of manipulating the chirality and polarity of topological magnetic states. Previously, vibrant research has shown that electrically switchable four FM skyrmions can be realized in multiferroic thin films [36,37]. Recently, many efforts have demonstrated that chiral domain walls and even skyrmions can be realized in FM multiferroic materials or FM-based multiferroic heterostructures [34,38–43]. In contrast, FM chiral textures can be tuned by external magnetic field, and antiferromagnetic (AFM) chiral spin textures are insensitive to magnetic field due to intrinsic lack of net magnetization. Realizing the effective manipulation and detection of spins stored in AFM materials is difficult based on common magnetic detectors [44,45]. Otherwise, electric-field control of AFM skyrmions is rarely reported. Excitingly, experimental progress has revealed that spins in AFM thin films can be manipulated by means of alternative internal field [46–48]. Additionally, it has been shown that AFM textures can be realized in multiferroic materials [33,49–51], and transformation between skyrmion and bimeron has recently been reported by controlling temperature or magnetic field [14,52]. Inspired by the experiments on strain-engineering magnetic parameters and magnetic orderings [23,53–56], we propose to realize colorful magnetic states via strain and electric-field control of chirality and polarity of tunable AFM textures in multiferroic materials.

In this letter, we propose the concept of switchable DMI and AFM skyrmions in type-I multiferroic oxide. Using first-principles calculations, we first present a theoretical study of magnetic parameters of $PbVO_3$ under continuous strain. The results of our simulations of an effective spin model with exchange parameters from *ab initio* calculations in $PbVO_3$ suggest that this material can host AFM skyrmions under different strain conditions [57,58]. Specifically, in contrast with vortex-antivortex pairs with relatively weaker in-plane magnetic anisotropy (IMA), the enhancement of compressive strain tends to form bimerons, while skyrmions can be stabilized under larger tensile strain. At last, using atomistic

*These authors contributed equally to this work.
†hongxin.yang@zju.edu.cn

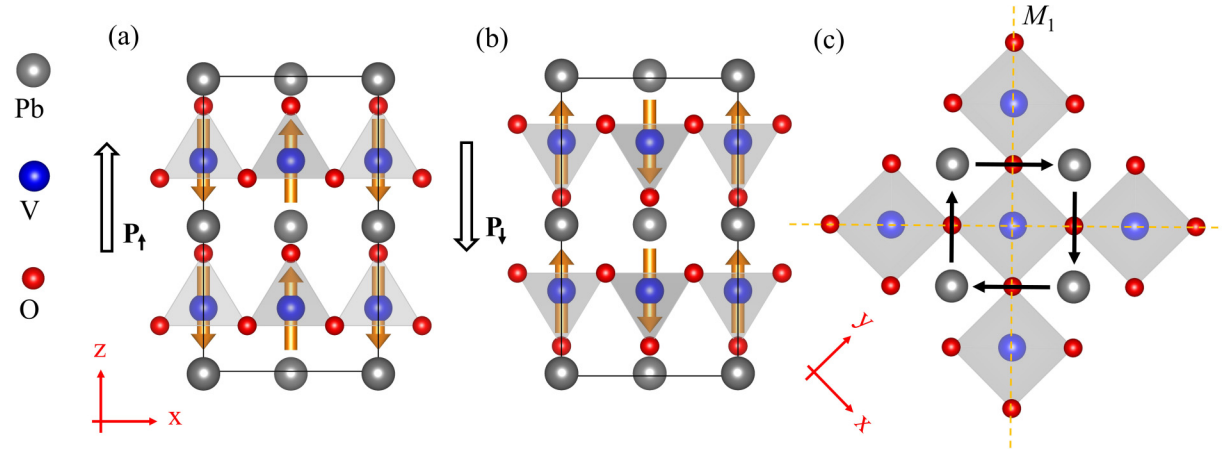

FIG. 1. (a) and (b) Ferroelectric *P*4*mm* phase of $PbVO_3$ with opposite polarizations, in which orange arrows are atomic magnetic moment and spin orientation. (c) Dyzaloshinskii-Moriya interaction (DMI) vectors (black arrows) between nearest-neighbor (NN) V atoms and M_1 indicate the mirror operations (orange dotted lines).

spin dynamics (ASD) simulations, four-state AFM skyrmions states (**P**↑,**L**↓), (**P**↑,**L**↑), (**P**↓,**L**↓), and (**P**↓,**L**↑) with different chirality and polarity are realized in multiferroic $PbVO_3$, where **P** and **L** represent the electric polarization and staggered magnetization $\mathbf{L} = (\mathbf{S}_i - \mathbf{S}_j)/2$ of FM sublattice pairs of AFM skyrmions ($\mathbf{S}_i$ and $\mathbf{S}_j$ are the nearest-neighboring (NN) spin pairs in skyrmion core [59]), respectively.

Concept. The energy dispersion $E_\sigma(\mathbf{k})$ of a given spin state is closely related to the symmetry of the system (σ and **k** indicate the spin up or down and wave vector). For a nonmagnetic paraelectric phase, it follows $E_\uparrow(\mathbf{k}) = E_\downarrow(-\mathbf{k})$ or $E_\downarrow(\mathbf{k}) = E_\uparrow(-\mathbf{k})$ arising from time-reversal symmetry (*T*) and $E_\uparrow(\mathbf{k}) = E_\uparrow(-\mathbf{k})$ or $E_\downarrow(\mathbf{k}) = E_\downarrow(-\mathbf{k})$ arising from inversion symmetry (*I*). Here, *I* is broken in a ferroelectric nonmagnetic system, SOC effect will induce so-called spin splitting at opposite wave vector **k** and −**k** points [$E_\uparrow(\mathbf{k}) \neq E_\uparrow(-\mathbf{k})$; $E_\downarrow(\mathbf{k}) \neq E_\downarrow(-\mathbf{k})$]. Instead, in a paraelectric FM system, the exchange field will lift degeneracy of energy dispersion [$E_\uparrow(\mathbf{k}) \neq E_\downarrow(-\mathbf{k})$ or $E_\downarrow(\mathbf{k}) \neq E_\uparrow(-\mathbf{k})$] due to the absence of *T*. The full breaking of *I* and *T* provides a sufficient condition to induce colorful spin textures. Strikingly, multiferroics simultaneously coexisting with ferroelectric and magnetic order can result in both *I* and *T* breaking, and thereby, four nondegenerate spin states will be induced. Electric-field control of ferroelectric polarization further can induce the full reversal of spin states [60–62]. The DMI effect is considered in multiferroics, where clockwise (CW) and anti-CW (ACW) chirality spin textures can be realized at opposite polarizations under certain conditions, respectively [36,37,63]. We put forward the concept in an AFM system, in which we have introduced four switchable AFM skyrmions (**P**↑,**L**↓), (**P**↑,**L**↑), (**P**↓,**L**↓), and (**P**↓,**L**↑), as is shown in Fig. S1 in the Supplemental Material [64]. More specifically, we focus on AFM multiferroic $PbVO_3$ that can realize AFM skrymions, discussed in detail below.

Results and discussion. Like perovskite ferroelectrics, e.g., $BaTiO_3$ and $PbTiO_3$, bulk $PbVO_3$ displays the polar crystal structure with the *P*4*mm* space group, which has been synthesized in experiments [58,65]. The top and side views of $PbVO_3$ crystal structure are presented in Figs. 1(a)–1(c), in which the orange arrows represent the magnetic orderings of the bulk phase. In our calculations, lattice constants are fixed to experimental values $a = b = 3.800$ Å and $c = 4.670$ Å. The ground states of $PbVO_3$ are calculated by considering four types of magnetic orderings (FM and A-, C-, and G-type AFM), as shown in Figs. S2(b)–S2(e) in the Supplemental Material [64]. The calculations show that the C-type AFM (Fig. S2(a) in the Supplemental Material [64]) is the ground state, which is consistent with experiment [65]. Furthermore, to explore the magnetic properties of studied systems, we adopt the following spin Hamiltonian:

$$H = -\sum_{\langle i,j\rangle} \mathbf{D}_{ij} \cdot (\mathbf{S}_i \times \mathbf{S}_j) - J_1 \sum_{\langle i,j\rangle} (\mathbf{S}_i \cdot \mathbf{S}_j) - J_2 \sum_{\langle i,j\rangle} (\mathbf{S}_i \cdot \mathbf{S}_j) - J_3 \sum_{\langle i,j\rangle} (\mathbf{S}_i \cdot \mathbf{S}_j) - K \sum_{\langle i\rangle} \left(S_i^z\right)^2,$$

where J_1, J_2, and J_3 are the intralayer NN, next-NN (NNN), and interlayer exchange coupling constants, respectively. Here, *K* and $\mathbf{D}_{ij}$ represent the magnetic anisotropy and DMI, respectively. ASD is used to explore the final chiral states by solving the Landau-Lifshitz-Gilbert equation, and magnetic parameters *J*, *K*, and *D* per magnetic atom are obtained by using DFT calculations. The computational details are given in the Supplemental Material [64].

First, we discuss the significant parameter *D* arising from the *I* breaking of the studied system. Bulk $PbVO_3$ has mirror operations M_1 passing through the NN V elements and vertical to the *xy* plane. According to the Moriya symmetry rules, there will be a DMI vector perpendicular to the NN magnetic atoms [see Fig. 1(c)] [17]. Additionally, one can see that the dominant energy contribution ΔE_{SOC} for the isotropic DMI vector stems from scattering of the heavy Pb element with strong SOC, as displayed in Fig. 2(b), like FM/HM interfaces [30,66,67], in which ΔE_{SOC} is mainly contributed by heavy 5*d* metal elements of the interfacial location. This is consistent with the Fert-Lévy mechanism of DMI [67,68]. In addition, Figs. 2(a) and S3 in the Supplemental Material [64] display the calculated spin-spiral energy $E(q)$ and DMI energy $\Delta E_{\mathrm{DMI}}(q)$ as a function of spin-spiral length *q* in the interval of *q* from $-\frac{\sqrt{2}}{2}(\frac{2\pi}{a})$ to $+\frac{\sqrt{2}}{2}(\frac{2\pi}{a})$ along the high-symmetry

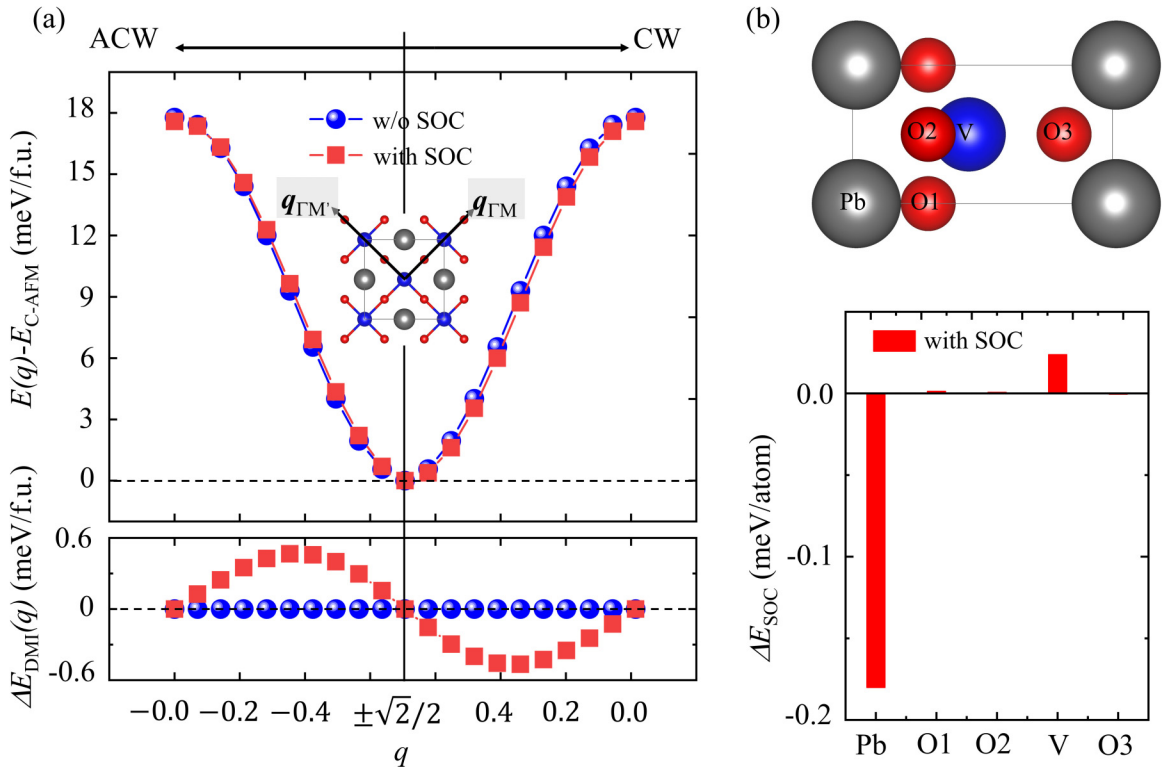

FIG. 2. (a) Spin spiral energy $E(q)$ (upper panel) and Dyzaloshinskii-Moriya interaction (DMI) energy $\Delta E_{\text{DMI}}(q)$ (lower panel) as functions of spin spiral length q for $PbVO_3$, in which E_{AFM} represents the energy of the antiferromagnetic (AFM) state at $q = \pm\frac{\sqrt{2}}{2}$. Red and blue points are calculated with and without (w/o) spin-orbit coupling (SOC), respectively. (b) Atom-resolved SOC energy ΔE_{SOC} at $q = \pm\frac{\sqrt{2}}{20}$, where one can clearly see that the energy source of SOC is dominated by the Pb atom.

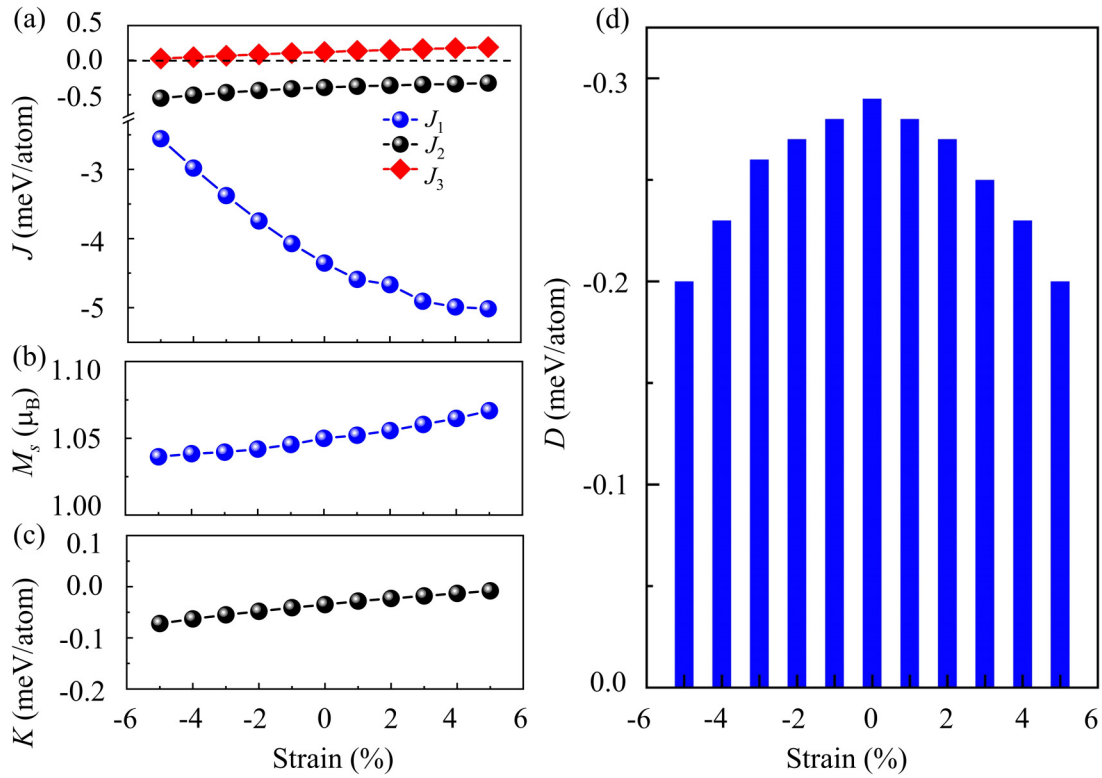

FIG. 3. The calculated (a) in-plane nearest-neighbor (NN), next-NN (NNN), and interlayer exchange coupling parameters J_1, J_2, and J_3, (b) magnetic moment M_s, (c) magnetic anisotropy K and Dyzaloshinskii-Moriya interaction (DMI) parameters D per V atom as functions of strain in multiferroic $PbVO_3$.

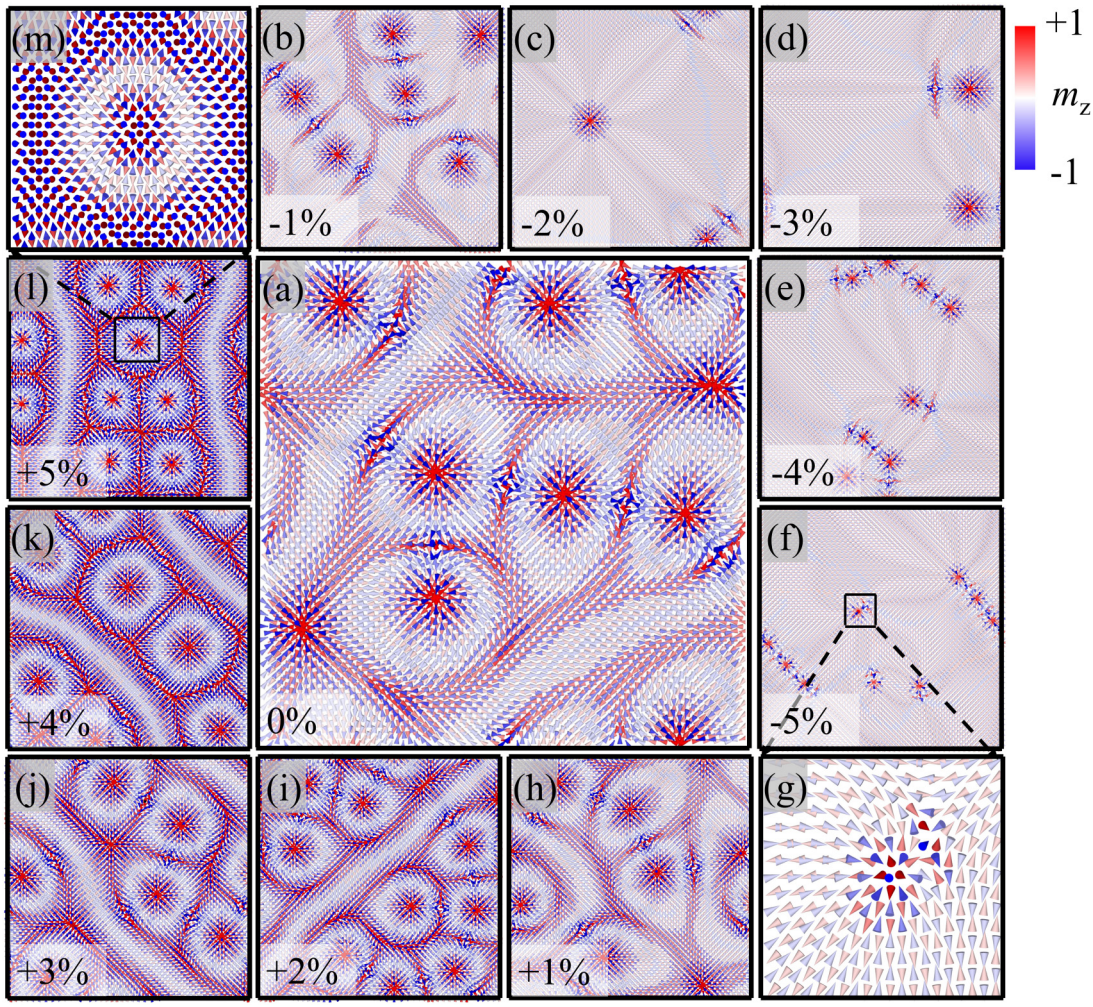

FIG. 4. (a)–(m) The evolution of spin textures with different strain varying from −5 to +5%. A complete transformation process of antiferromagnetic (AFM) skyrmion, vortex-antivortex pairs, and AFM bimeron as a function of strain in multiferroic $PbVO_3$.

Γ-*M* direction via performing the qSO method [69–71]. Not surprisingly, when SOC is neglected, calculated $E(q)$ and $\Delta E_{\mathrm{DMI}}(q)$ with $+q$ and $-q$ are degenerated [see the blue solid circles of Fig. 2(a)]. Once SOC is considered, energy dispersion $E(q)$ shows asymmetric behavior arising from DMI [see the red solid square of Fig. 2(a)]. Then from the linear fit of $\Delta E_{\mathrm{DMI}}(q)$ near the *M* point, the DMI parameters can be extracted by taking the slope of dispersion in the vicinity of the AFM ground state. It is worth noting that the real-space spin-spiral method further confirms the reliability of our results [67]; details are in the Supplemental Material [64]. Otherwise, notice that the magnetic anisotropy of bulk $PbVO_3$ is very small, which is the consequence of Kramers degeneracy for the odd-electron systems, as depicted in previous reports [72,73]. We also estimate the in-plane NN, NNN, and interlayer exchange constants J_1, J_2, and J_3. Calculated results indicate that the magnitudes of J_1 are much larger than J_2 and J_3, as shown in Fig. 3(a). Otherwise, J_1 and J_2 are AFM coupling, which indicates the possibility of in-plane spin frustration [74–76]. Figure S4 in the Supplemental Material [64] further displays the ratio of J_2/J_1 as a function of strain; we can see that J_2/J_1 evidently decreases as the strain rises from −5 to +5%. Finally, we perform ASD simulations to explore the possibility of topological magnetism from the above magnetic parameters. Clearly, one can see that vortex-antivortex pairs will emerge [Fig. 4(a)] due to the weak IMA. Once the IMA is increased (decreased), bimerons (skyrmions) can be realized in this multiferroic oxide, and detailed discussion follows.

Transformation of AFM skyrmions-AFM vortex and antivortex pairs-AFM bimerons. With the help of ASD simulations, AFM spin textures in real space corresponding to different strains are displayed as shown in Fig. 4. In the strain ranging from 0 to −5%, one can see that topological spin texture evolutes from vortex-antivortex pairs to isolated bimerons and further transforms into a bimeron chain. For the initial state, we can understand that the loops of vortexes and antivortexes arise from the result of interplay between exchange coupling and DMI within weak IMA, which is consistent with previous results, e.g., In_2Se_3/La_2Cl_2 ($K = -0.06$ meV) and Janus $MnBi_2Se_2Te_2$ ($K = 0.006$ meV) [77,78]. Next, we find that IMA can effectively improve with the compressive strain varying from 0 to −5% and the ratio of D/J_1 retains roughly constant (see Fig. S16 in the Supplemental Material [64]), where the chiral spin texture can evolute from vortex-antivortex pairs to bimerons and further transform into a bimeron chain. The above results are like In_2Se_3/La_2Cl_2,

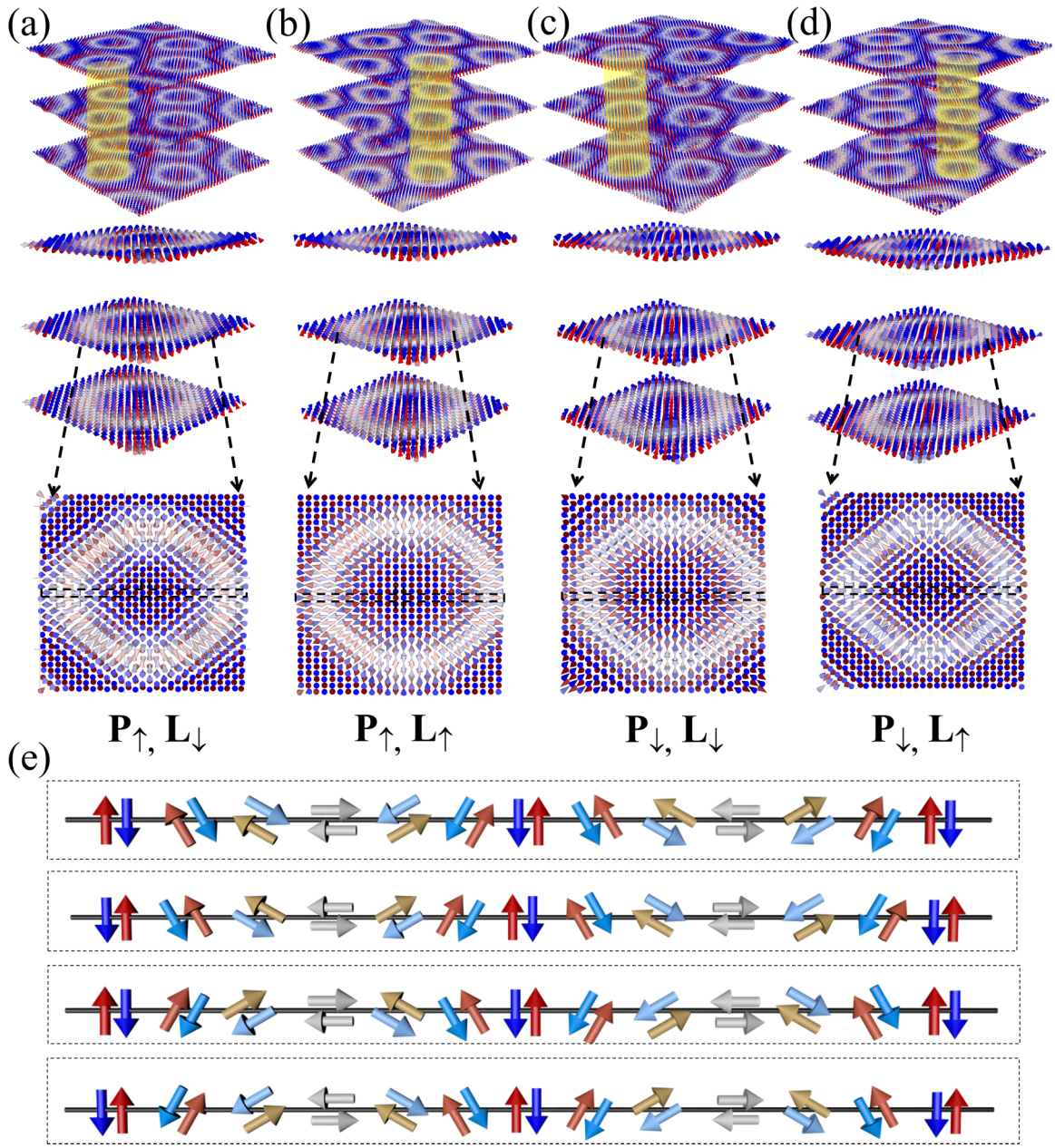

FIG. 5. (a)–(d) The realization of four-state antiferromagnetic (AFM) skyrmions ($\mathbf{P}\uparrow$,$\mathbf{L}\downarrow$), ($\mathbf{P}\uparrow$,$\mathbf{L}\uparrow$), ($\mathbf{P}\downarrow$,$\mathbf{L}\downarrow$), and ($\mathbf{P}\downarrow$,$\mathbf{L}\uparrow$) with different chirality and polarity. Here, $\mathbf{P}$ and $\mathbf{L}$ represent the electric polarization and staggered magnetization $\mathbf{L} = (\mathbf{S}_i - \mathbf{S}_j)/2$ of ferromagnetic sublattice pairs of AFM skyrmion ($\mathbf{S}_i$ and $\mathbf{S}_j$ are the nearest-neighboring spins), respectively. (e) Cycloidal spin spirals with AFM short-range orders corresponding to above four-state skyrmions propagate with wave vector $\mathbf{q}$ along the x direction.

where the increasing easy-plane anisotropy will result in the transformation between vortex-antivortex pairs and bimerons. Meanwhile, we can find the existence of isolated merons with the increase of IMA [Fig. 4(c)]. Such spin textures with a half-quantized skyrmion number $Q = \frac{1}{2}$ have also been reported in chiral magnets with easy-plane anisotropy [79,80]. Additionally, we calculate the topological distribution of $PbVO_3$ in strain varying from 0 to -5%. The Q of meron and antimeron are all $-\frac{1}{2}$, and the Q of an isolate bimeron composed of them is -1, as shown in Fig. S6 in the Supplemental Material [64].

Meanwhile, we find that the formation of Néel skyrmions can appear under strain varying from 0 to $+5\%$. Figures 4(h)–4(l) represent the skyrmion textures gradually emerging when the IMA is decreased to a relatively lower value [see Fig. 3(c)]. Meanwhile, in the zoomed AFM skyrmion, as shown in Fig. 4(m), two FM sublattices with opposite topological charges Q can be observed. This will lead to the AFM skyrmion moving parallel to the applied current direction without showing the skyrmion Hall effect [81–83]. As shown in Fig. S6 in the Supplemental Material [64], one can see that the skyrmion numbers under $+5\%$ tensile strain are equal to -5, which is consistent with the results from calculation of the topological charge. In addition, the influence of temperature effects on the magnetic structure is further considered, and the details are described in the Supplemental Material [64].

More specifically, we summarize the diagrams of magnetic textures of one and three layers as a function of strain in Figs. 4 and S5 in the Supplemental Material [64], respectively. Clearly, a complete evolution of skyrmion to vortex and antivortex pairs to bimeron spin textures is shown. In contrast, authors of previous works have reported on transition of topological magnetism by controlling temperature or magnetic field [14,84]. However, an ideal transition between an AFM skyrmion and an AFM bimeron has not been reported. Our results present an interesting transition between an AFM skyrmion and an AFM bimeron, which is helpful for us to design AFM-skyrmion-based memory devices.

In addition, it has been unveiled that strain-dependent magnetic textures can be obtained by an epitaxial substrate in ultrathin oxides [38,56,85,86]. To demonstrate strain-engineered AFM skyrmions in similar heterostructures, we construct ultrathin $PbVO_3/BaTiO_3$ and $PbVO_3/SrTiO_3$ heterostructures (Fig. S21 in the Supplemental Material [64]). We find that AFM skyrmions can still be realized in ultrathin heterostructures through using ASD simulations, as shown in Fig. S22 in the Supplemental Material [64]. These results sufficiently prove the existence of AFM skyrmions in $PbVO_3$. Additionally, the multiferroic structure, which has opposite DMI chirality, provides the possibility of manipulating the chirality of topological magnetic states by electric field. As shown in Fig. S12 in the Supplemental Material [64], we have investigated the ferroelectric switching pathway by using the climbing-image nudged elastic band (CI-NEB) method [87], where the ferroelectric phase corresponding to polarization down $\mathbf{P}\downarrow$ first converts into a transition state and moves further from the transition state back to the ferroelectric phase with opposite polarization up $\mathbf{P}\uparrow$. With the reversal of polarization in multiferroic $PbVO_3$ by an out-of-plane electric field, the chirality of DMI can be switched. Meanwhile, we perform ASD for ferroelectric phases ($\mathbf{P}\uparrow$ and $\mathbf{P}\downarrow$) and calculate the numerical energy of these states; one can clearly see that the total energy of AFM skyrmions for ferroelectric phases are basically the same (see Fig. S13 in the Supplemental Material [64]). Like previous reports on multiferroic CrN and $Co(MoS_2)_2$ [36,37,88], we relax from a random state [or FM and C- and G-type AFM, and spin-spiral states (see Figs. S14 and S15 in the Supplemental Material [64])] to obtain four-state AFM skyrmions ($\mathbf{P}\uparrow$,$\mathbf{L}\downarrow$), ($\mathbf{P}\uparrow$,$\mathbf{L}\uparrow$), ($\mathbf{P}\downarrow$,$\mathbf{L}\downarrow$), and ($\mathbf{P}\downarrow$,$\mathbf{L}\uparrow$) with different chirality and polarity via applying 5% tensile strain in bulk $PbVO_3$ (see Fig. 5). Our findings provide a platform to investigate electric-field control chirality and polarity of AFM skyrmions, which is useful for potential application of future devices.

Conclusions. In conclusion, we propose that the chirality and polarity of AFM skyrmions can be controlled in multiferroic oxides. Using first-principles calculations and ASD simulations, we unveil the process of phase transformation of AFM bimerons, AFM vortex-antivortex pairs, and AFM skyrmions in $PbVO_3$. Moreover, we demonstrate that AFM skrymions can be realized in multiferroic $PbVO_3$ and even its ultrathin heterostructures based on strain-mediated phase engineering. Finally, we show that four-state AFM skyrmions, i.e., ($\mathbf{P}\uparrow$,$\mathbf{L}\downarrow$), ($\mathbf{P}\uparrow$,$\mathbf{L}\uparrow$), ($\mathbf{P}\downarrow$,$\mathbf{L}\downarrow$), and ($\mathbf{P}\downarrow$,$\mathbf{L}\uparrow$) with different chirality and polarity, can be realized in $PbVO_3$ via external electric field. Our results provide a highly promising approach to control the AFM topological spin textures in multiferroic compounds.

Acknowledgments. This letter was supported by the "Pioneer" and "Leading Goose" R&D Program of Zhejiang Province (Grant No. 2022C01053), the National Key Research and Development Program of China (Grants No. 2022YFA1405100 and No. 2022YFA1403601), the National Natural Science Foundation of China (Grants No. 12174405 and No. 12204497), Ningbo Key Scientific and Technological Project (Grant No. 2021000215).

[1] A. Fert, N. Reyren, and V. Cros, Magnetic skyrmions: Advances in physics and potential applications, Nat. Rev. Mater. **2**, 17031 (2017).

[2] Y. H. Chu, L. W. Martin, M. B. Holcomb, M. Gajek, S. J. Han, Q. He, N. Balke, C. H. Yang, D. Lee, W. Hu *et al.*, Electric-field control of local ferromagnetism using a magnetoelectric multiferroic, Nat. Mater. **7**, 478 (2008).

[3] M. Bibes and A. Barthélémy, Towards a magnetoelectric memory, Nat. Mater. **7**, 425 (2008).

[4] F. Matsukura, Y. Tokura, and H. Ohno, Control of magnetism by electric fields, Nat. Nanotechnol. **10**, 209 (2015).

[5] A. C. Garcia-Castro, W. Ibarra-Hernandez, E. Bousquet, and A. H. Romero, Direct magnetization-polarization coupling in $BaCuF_4$, Phys. Rev. Lett. **121**, 117601 (2018).

[6] C. G. Duan, J. P. Velev, R. F. Sabirianov, Z. Zhu, J. Chu, S. S. Jaswal, and E. Y. Tsymbal, Surface magnetoelectric effect in ferromagnetic metal films, Phys. Rev. Lett. **101**, 137201 (2008).

[7] M. Gajek, M. Bibes, S. Fusil, K. Bouzehouane, J. Fontcuberta, A. Barthelemy, and A. Fert, Tunnel junctions with multiferroic barriers, Nat. Mater. **6**, 296 (2007).

[8] S. H. Chun, Y. S. Chai, B. G. Jeon, H. J. Kim, Y. S. Oh, I. Kim, H. Kim, B. J. Jeon, S. Y. Haam, J. Y. Park *et al.*, Electric field control of nonvolatile four-state magnetization at room temperature, Phys. Rev. Lett. **108**, 177201 (2012).

[9] L. Ponet, S. Artyukhin, T. Kain, J. Wettstein, A. Pimenov, A. Shuvaev, X. Wang, S. W. Cheong, M. Mostovoy, and A. Pimenov, Topologically protected magnetoelectric switching in a multiferroic, Nature (London) **607**, 81 (2022).

[10] B. Dieny, I. L. Prejbeanu, K. Garello, P. Gambardella, P. Freitas, R. Lehndorff, W. Raberg, U. Ebels, S. O. Demokritov, J. Akerman *et al.*, Opportunities and challenges for spintronics in the microelectronics industry, Nat. Electron. **3**, 446 (2020).

[11] A. Thiaville, S. Rohart, É. Jué, V. Cros, and A. Fert, Dynamics of Dzyaloshinskii domain walls in ultrathin magnetic films, Europhys. Lett. **100**, 57002 (2012).

[12] A. N. Bogdanov and D. Yablonskii, Thermodynamically stable "vortices" in magnetically ordered crystals. The mixed state of magnets, Sov. Phys. JETP **68**, 101 (1989).

[13] X. Z. Yu, N. Kanazawa, Y. Onose, K. Kimoto, W. Z. Zhang, S. Ishiwata, Y. Matsui, and Y. Tokura, Near room-temperature

formation of a skyrmion crystal in thin-films of the helimagnet FeGe, Nat. Mater. **10**, 106 (2011).
[14] H. Jani, J. C. Lin, J. Chen, J. Harrison, F. Maccherozzi, J. Schad, S. Prakash, C. B. Eom, A. Ariando, T. Venkatesan *et al.*, Antiferromagnetic half-skyrmions and bimerons at room temperature, Nature (London) **590**, 74 (2021).
[15] B. Göbel, A. Mook, J. Henk, I. Mertig, and O. A. Tretiakov, Magnetic bimerons as skyrmion analogues in in-plane magnets, Phys. Rev. B **99**, 060407(R) (2019).
[16] I. Dzyaloshinsky, A thermodynamic theory of "weak" ferromagnetism of antiferromagnetics, J. Phys. Chem. Solids **4**, 241 (1958).
[17] T. Moriya, Anisotropic superexchange interaction and weak ferromagnetism, Phys. Rev. **120**, 91 (1960).
[18] M. Kuepferling, A. Casiraghi, G. Soares, G. Durin, F. Garcia-Sanchez, L. Chen, C. H. Back, C. H. Marrows, S. Tacchi, and G. Carlotti, Measuring interfacial Dzyaloshinskii-Moriya interaction in ultrathin magnetic films, Rev. Mod. Phys. **95**, 015003 (2023).
[19] T. Kimura, T. Goto, H. Shintani, K. Ishizaka, T. Arima, and Y. Tokura, Magnetic control of ferroelectric polarization, Nature (London) **426**, 55 (2003).
[20] N. A. Spaldin and M. Fiebig, The renaissance of magnetoelectric multiferroics, Science **309**, 391 (2005).
[21] S. Luo, M. Song, X. Li, Y. Zhang, J. Hong, X. Yang, X. Zou, N. Xu, and L. You, Reconfigurable skyrmion logic gates, Nano Lett. **18**, 1180 (2018).
[22] A. Fert, V. Cros, and J. Sampaio, Skyrmions on the track, Nat. Nanotechnol. **8**, 152 (2013).
[23] H. Yan, Z. Feng, S. Shang, X. Wang, Z. Hu, J. Wang, Z. Zhu, H. Wang, Z. Chen, H. Hua *et al.*, Strain-controlled antiferromagnetic memory insensitive to magnetic fields, Nat. Nanotechnol. **14**, 131 (2019).
[24] D. Yu, H. Yang, M. Chshiev, and A. Fert, Skyrmions-based logic gates in one single nanotrack completely reconstructed via chirality barrier, Nat. Sci. Rev. **9**, nwac021 (2022).
[25] S. Mühlbauer, B. Binz, F. Jonietz, C. Pfleiderer, A. Rosch, A. Neubauer, R. Georgii, and P. Böni, Skyrmion lattice in a chiral magnet, Science **323**, 915 (2009).
[26] X. Z. Yu, Y. Onose, N. Kanazawa, J. H. Park, J. H. Han, Y. Matsui, N. Nagaosa, and Y. Tokura, Real-space observation of a two-dimensional skyrmion crystal, Nature (London) **465**, 901 (2010).
[27] S. Heinze, K. von Bergmann, M. Menzel, J. Brede, A. Kubetzka, R. Wiesendanger, G. Bihlmayer, and S. Blügel, Spontaneous atomic-scale magnetic skyrmion lattice in two dimensions, Nat. Phys. **7**, 713 (2011).
[28] L. Wang, Y. Ga, Q. Cui, P. Li, J. Liang, Y. Zhou, S. Wang, and H. Yang, Oxidization engineered Dzyaloshinskii-Moriya interaction and topological magnetism at Fe/MgO bilayers, Phys. Rev. B **108**, 214404 (2023).
[29] W. Jiang, P. Upadhyaya, W. Zhang, G. Yu, M. B. Jungfleisch, F. Y. Fradin, J. E. Pearson, Y. Tserkovnyak, K. L. Wang, O. Heinonen *et al.*, Blowing magnetic skyrmion bubbles, Science **349**, 283 (2015).
[30] O. Boulle, J. Vogel, H. Yang, S. Pizzini, D. de Souza Chaves, A. Locatelli, T. O. Mentes, A. Sala, L. D. Buda-Prejbeanu, O. Klein *et al.*, Room-temperature chiral magnetic skyrmions in ultrathin magnetic nanostructures, Nat. Nanotechnol. **11**, 449 (2016).
[31] A. K. Nayak, V. Kumar, T. Ma, P. Werner, E. Pippel, R. Sahoo, F. Damay, U. K. Rossler, C. Felser, and S. S. P. Parkin, Magnetic antiskyrmions above room temperature in tetragonal Heusler materials, Nature (London) **548**, 561 (2017).
[32] K. Karube, L. Peng, J. Masell, X. Yu, F. Kagawa, Y. Tokura, and Y. Taguchi, Room-temperature antiskyrmions and sawtooth surface textures in a non-centrosymmetric magnet with S4 symmetry, Nat. Mater. **20**, 335 (2021).
[33] T. Zhao, A. Scholl, F. Zavaliche, K. Lee, M. Barry, A. Doran, M. P. Cruz, Y. H. Chu, C. Ederer, N. A. Spaldin *et al.*, Electrical control of antiferromagnetic domains in multiferroic $BiFeO_3$ films at room temperature, Nat. Mater. **5**, 823 (2006).
[34] S. Seki, X. Z. Yu, S. Ishiwata, and Y. Tokura, Observation of skyrmions in a multiferroic material, Science **336**, 198 (2012).
[35] J. F. Scott, Room-temperature multiferroic magnetoelectrics, NPG Asia Mater. **5**, e72 (2013).
[36] Z. Shao, J. Liang, Q. Cui, M. Chshiev, A. Fert, T. Zhou, and H. Yang, Multiferroic materials based on transition-metal dichalcogenides: Potential platform for reversible control of Dzyaloshinskii-Moriya interaction and skyrmion via electric field, Phys. Rev. B **105**, 174404 (2022).
[37] J. Liang, Q. Cui, and H. Yang, Electrically switchable Rashba-type Dzyaloshinskii-Moriya interaction and skyrmion in two-dimensional magnetoelectric multiferroics, Phys. Rev. B **102**, 220409(R) (2020).
[38] Y. Ba, S. Zhuang, Y. Zhang, Y. Wang, Y. Gao, H. Zhou, M. Chen, W. Sun, Q. Liu, G. Chai *et al.*, Electric-field control of skyrmions in multiferroic heterostructure via magnetoelectric coupling, Nat. Commun. **12**, 322 (2021).
[39] Y. Wang, J. Sun, T. Shimada, H. Hirakata, T. Kitamura, and J. Wang, Ferroelectric control of magnetic skyrmions in multiferroic heterostructures, Phys. Rev. B **102**, 014440 (2020).
[40] L. Wang, Q. Feng, Y. Kim, R. Kim, K. H. Lee, S. D. Pollard, Y. J. Shin, H. Zhou, W. Peng, D. Lee *et al.*, Ferroelectrically tunable magnetic skyrmions in ultrathin oxide heterostructures, Nat. Mater. **17**, 1087 (2018).
[41] N. Leo, A. Bergman, A. Cano, N. Poudel, B. Lorenz, M. Fiebig, and D. Meier, Polarization control at spin-driven ferroelectric domain walls, Nat. Commun. **6**, 6661 (2015).
[42] R. O. Cherifi, V. Ivanovskaya, L. C. Phillips, A. Zobelli, I. C. Infante, E. Jacquet, V. Garcia, S. Fusil, P. R. Briddon, N. Guiblin *et al.*, Electric-field control of magnetic order above room temperature, Nat. Mater. **13**, 345 (2014).
[43] Y. Tokunaga, N. Furukawa, H. Sakai, Y. Taguchi, T. H. Arima, and Y. Tokura, Composite domain walls in a multiferroic perovskite ferrite, Nat. Mater. **8**, 558 (2009).
[44] T. Jungwirth, X. Marti, P. Wadley, and J. Wunderlich, Antiferromagnetic spintronics, Nat. Nanotechnol. **11**, 231 (2016).
[45] A. MacDonald and M. Tsoi, Antiferromagnetic metal spintronics, Philos. Trans. R. Soc. A **369**, 3098 (2011).
[46] P. Wadley, B. Howells, J. Železný, C. Andrews, V. Hills, R. P. Campion, V. Novák, K. Olejník, F. Maccherozzi, S. S. Dhesi *et al.*, Electrical switching of an antiferromagnet, Science **351**, 587 (2016).
[47] O. J. Amin, S. F. Poole, S. Reimers, L. X. Barton, A. Dal Din, F. Maccherozzi, S. S. Dhesi, V. Novak, F. Krizek, J. S. Chauhan *et al.*, Antiferromagnetic half-skyrmions electrically generated and controlled at room temperature, Nat. Nanotechnol. (2023).

[48] X. Chen, H. Bai, Y. Ji, Y. Zhou, L. Liao, Y. You, W. Zhu, Q. Wang, L. Han, X. Liu *et al.*, Control of spin current and antiferromagnetic moments via topological surface state, Nat. Electron. **5**, 574 (2022).

[49] A. Finco, A. Haykal, S. Fusil, P. Kumar, P. Dufour, A. Forget, D. Colson, J. Y. Chauleau, M. Viret, N. Jaouen *et al.*, Imaging topological defects in a noncollinear antiferromagnet, Phys. Rev. Lett. **128**, 187201 (2022).

[50] J. Y. Chauleau, T. Chirac, S. Fusil, V. Garcia, W. Akhtar, J. Tranchida, P. Thibaudeau, I. Gross, C. Blouzon, A. Finco *et al.*, Electric and antiferromagnetic chiral textures at multiferroic domain walls, Nat. Mater. **19**, 386 (2020).

[51] D. M. Evans, V. Garcia, D. Meier, and M. Bibes, Domains and domain walls in multiferroics, Phys. Sci. Rev. **5**, 20190067 (2020).

[52] K. Ohara, X. Zhang, Y. Chen, S. Kato, J. Xia, M. Ezawa, O. A. Tretiakov, Z. Hou, Y. Zhou, G. Zhao *et al.*, Reversible transformation between isolated skyrmions and bimerons, Nano Lett. **22**, 8559 (2022).

[53] M. P. Cruz, Y. H. Chu, J. X. Zhang, P. L. Yang, F. Zavaliche, Q. He, P. Shafer, L. Q. Chen, and R. Ramesh, Strain control of domain-wall stability in epitaxial $BiFeO_3$ (110) films, Phys. Rev. Lett. **99**, 217601 (2007).

[54] H. S. Kum, H. Lee, S. Kim, S. Lindemann, W. Kong, K. Qiao, P. Chen, J. Irwin, J. H. Lee, S. Xie *et al.*, Heterogeneous integration of single-crystalline complex-oxide membranes, Nature (London) **578**, 75 (2020).

[55] S. S. Hong, M. Gu, M. Verma, V. Harbola, B. Y. Wang, D. Lu, A. Vailionis, Y. Hikita, R. Pentcheva, J. M. Rondinelli *et al.*, Extreme tensile strain states in $La_{0.7}Ca_{0.3}MnO_3$ membranes, Science **368**, 71 (2020).

[56] A. Haykal, J. Fischer, W. Akhtar, J. Y. Chauleau, D. Sando, A. Finco, F. Godel, Y. A. Birkholzer, C. Carretero, N. Jaouen *et al.*, Antiferromagnetic textures in $BiFeO_3$ controlled by strain and electric field, Nat. Commun. **11**, 1704 (2020).

[57] R. V. Shpanchenko, V. V. Chernaya, A. A. Tsirlin, P. S. Chizhov, D. E. Sklovsky, E. V. Antipov, E. P. Khlybov, V. Pomjakushin, A. M. Balagurov, J. E. Medvedeva *et al.*, Synthesis, structure, and properties of new perovskite $PbVO_3$, Chem. Mater. **16**, 3267 (2004).

[58] L. W. Martin, Q. Zhan, Y. Suzuki, R. Ramesh, M. Chi, N. Browning, T. Mizoguchi, and J. Kreisel, Growth and structure of $PbVO_3$ thin films, App. Phys. Lett. **90**, 062903 (2007).

[59] N. Nagaosa and Y. Tokura, Topological properties and dynamics of magnetic skyrmions, Nat. Nanotechnol. **8**, 899 (2013).

[60] M. Kawano, Y. Onose, and C. Hotta, Designing Rashba-Dresselhaus effect in magnetic insulators, Commun. Phys. **2**, 27 (2019).

[61] D. Di Sante, P. Barone, R. Bertacco, and S. Picozzi, Electric control of the giant Rashba effect in bulk GeTe, Adv. Mater. **25**, 509 (2013).

[62] S. Picozzi, Ferroelectric Rashba semiconductors as a novel class of multifunctional materials, Front. Phys. **2**, 10 (2014).

[63] C. Xu, P. Chen, H. Tan, Y. Yang, H. Xiang, and L. Bellaiche, Electric-field switching of magnetic topological charge in type-I multiferroics, Phys. Rev. Lett. **125**, 037203 (2020).

[64] See Supplemental Material at http://link.aps.org/supplemental/10.1103/PhysRevB.109.L060402 for (i) computational details for first-principles calculations, (ii) details of ASD simulations, (iii) computational details for magnetic parameters, (iv) theoretical analysis and calculations for ultrathin oxide heterostructures, (v) evolution of the magnetic parameters under an electric field, (vi) calculated topological charge under different strain, (vii) different initial states on the influence of final spin textures, and (viii) the influence of the thermal effects on spin texture, which includes Refs. [23,37,40,55,56,59,67,69,74,81,89–106].

[65] K. Oka, I. Yamada, M. Azuma, S. Takeshita, K. H. Satoh, A. Koda, R. Kadono, M. Takano, and Y. Shimakawa, Magnetic ground-state of perovskite $PbVO_3$ with large tetragonal distortion, Inorg. Chem. **47**, 7355 (2008).

[66] B. Dupe, M. Hoffmann, C. Paillard, and S. Heinze, Tailoring magnetic skyrmions in ultra-thin transition metal films, Nat. Commun. **5**, 4030 (2014).

[67] H. Yang, A. Thiaville, S. Rohart, A. Fert, and M. Chshiev, Anatomy of Dzyaloshinskii-Moriya interaction at Co/Pt interfaces, Phys. Rev. Lett. **115**, 267210 (2015).

[68] A. Fert and P. M. Levy, Role of anisotropic exchange interactions in determining the properties of spin-glasses, Phys. Rev. Lett. **44**, 1538 (1980).

[69] L. M. Sandratskii, Insight into the Dzyaloshinskii-Moriya interaction through first-principles study of chiral magnetic structures, Phys. Rev. B **96**, 024450 (2017).

[70] M. Heide, G. Bihlmayer, and S. Blügel, Describing Dzyaloshinskii-Moriya spirals from first principles, Phys. B: Condens. Matter **404**, 2678 (2009).

[71] H. Yang, J. Liang, and Q. Cui, First-principles calculations for Dzyaloshinskii-Moriya interaction, Nat. Rev. Phys. **5**, 43 (2023).

[72] I. V. Solovyev, Magnetic structure of the noncentrosymmetric perovskites $PbVO_3$ and $BiCoO_3$: Theoretical analysis, Phys. Rev. B **85**, 054420 (2012).

[73] A. Diaz-Bachs, M. I. Katsnelson, and A. Kirilyuk, Kramers degeneracy and relaxation in vanadium, niobium and tantalum clusters, New J. Phys. **20**, 043042 (2018).

[74] A. A. Tsirlin, A. A. Belik, R. V. Shpanchenko, E. V. Antipov, E. Takayama-Muromachi, and H. Rosner, Frustrated spin-$\frac{1}{2}$ square lattice in the layered perovskite $PbVO_3$, Phys. Rev. B **77**, 092402 (2008).

[75] B. Xu, S. Meyer, M. J. Verstraete, L. Bellaiche, and B. Dupé, First-principles study of spin spirals in the multiferroic $BiFeO_3$, Phys. Rev. B **103**, 214423 (2021).

[76] S. Meyer, M. Perini, S. von Malottki, A. Kubetzka, R. Wiesendanger, K. von Bergmann, and S. Heinze, Isolated zero field sub-10 nm skyrmions in ultrathin Co films, Nat. Commun. **10**, 3823 (2019).

[77] W. Sun, W. Wang, H. Li, G. Zhang, D. Chen, J. Wang, and Z. Cheng, Controlling bimerons as skyrmion analogues by ferroelectric polarization in 2D van der Waals multiferroic heterostructures, Nat. Commun. **11**, 5930 (2020).

[78] Q. Cui, Y. Zhu, J. Jiang, J. Liang, D. Yu, P. Cui, and H. Yang, Ferroelectrically controlled topological magnetic phase in a Janus-magnet-based multiferroic heterostructure, Phys. Rev. Res. **3**, 043011 (2021).

[79] S.-Z. Lin, A. Saxena, and C. D. Batista, Skyrmion fractionalization and merons in chiral magnets with easy-plane anisotropy, Phys. Rev. B **91**, 224407 (2015).

[80] D. Bachmann, M. Lianeris, and S. Komineas, Meron configurations in easy-plane chiral magnets, Phys. Rev. B **108**, 014402 (2023).

[81] X. Zhang, Y. Zhou, and M. Ezawa, Antiferromagnetic skyrmion: Stability, creation and manipulation, Sci. Rep. **6**, 24795 (2016).

[82] W. Jiang, X. Zhang, G. Yu, W. Zhang, X. Wang, M. B. Jungfleisch, J. E. Pearson, X. Cheng, O. Heinonen, K. L. Wang *et al.*, Direct observation of the skyrmion Hall effect, Nat. Phys. **13**, 162 (2016).

[83] J. Barker and O. A. Tretiakov, Static and dynamical properties of antiferromagnetic skyrmions in the presence of applied current and temperature, Phys. Rev. Lett. **116**, 147203 (2016).

[84] X. Z. Yu, W. Koshibae, Y. Tokunaga, K. Shibata, Y. Taguchi, N. Nagaosa, and Y. Tokura, Transformation between meron and skyrmion topological spin textures in a chiral magnet, Nature (London) **564**, 95 (2018).

[85] D. Ji, S. Cai, T. R. Paudel, H. Sun, C. Zhang, L. Han, Y. Wei, Y. Zang, M. Gu, Y. Zhang *et al.*, Freestanding crystalline oxide perovskites down to the monolayer limit, Nature (London) **570**, 87 (2019).

[86] D. Sando, B. Xu, L. Bellaiche, and V. Nagarajan, A multiferroic on the brink: Uncovering the nuances of strain-induced transitions in $BiFeO_3$, Appl. Phys. Rev. **3**, 011106 (2016).

[87] G. Henkelman, B. P. Uberuaga, and H. Jónsson, A climbing image nudged elastic band method for finding saddle points and minimum energy paths, J. Chem. Phys. **113**, 9901 (2000).

[88] D. Yu, Y. Ga, J. Liang, C. Jia, and H. Yang, Voltage-controlled Dzyaloshinskii-Moriya interaction torque switching of perpendicular magnetization, Phys. Rev. Lett. **130**, 056701 (2023).

[89] G. Kresse and J. Furthmüller, Efficient iterative schemes for *ab initio* total-energy calculations using a plane-wave basis set, Phys. Rev. B **54**, 11169 (1996).

[90] J. P. Perdew, K. Burke, and M. Ernzerhof, Generalized gradient approximation made simple, Phys. Rev. Lett. **77**, 3865 (1996).

[91] G. Kresse and J. Hafner, *Ab initio* molecular dynamics for liquid metals, Phys. Rev. B **47**, 558 (1993).

[92] G. Kresse and J. Furthmüller, Efficiency of *ab initio* total energy calculations for metals and semiconductors using a plane-wave basis set, Comput. Mater. Sci. **6**, 15 (1996).

[93] I. A. Vladimir, F. Aryasetiawan, and A. I. Lichtenstein, First-principles calculations of the electronic structure and spectra of strongly correlated systems: The LDA+U method, J. Phys.: Condens. Matter **9**, 767 (1997).

[94] K. Oka, T. Yamauchi, S. Kanungo, T. Shimazu, K. Oh-ishi, Y. Uwatoko, M. Azuma, and T. Saha-Dasgupta, Experimental and theoretical studies of the metallic conductivity in cubic $PbVO_3$ under high pressure, J. Phys. Soc. Japan **87**, 024801 (2018).

[95] B. Skubic, J. Hellsvik, L. Nordström, and O. Eriksson, A method for atomistic spin dynamics simulations: Implementation and examples, J. Phys.: Condens. Matter **20**, 315203 (2008).

[96] H. J. Xiang, E. J. Kan, S.-H. Wei, M. H. Whangbo, and X. G. Gong, Predicting the spin-lattice order of frustrated systems from first principles, Phys. Rev. B **84**, 224429 (2011).

[97] J. Liang, W. Wang, H. Du, A. Hallal, K. Garcia, M. Chshiev, A. Fert, and H. Yang, Very large Dzyaloshinskii-Moriya interaction in two-dimensional Janus manganese dichalcogenides and its application to realize skyrmion states, Phys. Rev. B **101**, 184401 (2020).

[98] S. Zhou, L. Liao, L. Chen, B. Feng, X. He, X. Bai, C. Song, and K. Wu, Ferroelectricity in epitaxial perovskite oxide Bi_2WO_6 films with one-unit-cell thickness, Nano Lett. **23**, 7838 (2023).

[99] J. Junquera and P. Ghosez, Critical thickness for ferroelectricity in perovskite ultrathin films, Nature (London) **422**, 506 (2003).

[100] S. S. Cheema, D. Kwon, N. Shanker, R. dos Reis, S.-L. Hsu, J. Xiao, H. Zhang, R. Wagner, A. Datar, M. R. McCarter *et al.*, Enhanced ferroelectricity in ultrathin films grown directly on silicon, Nature (London) **580**, 478 (2020).

[101] J. Matsuno, N. Ogawa, K. Yasuda, F. Kagawa, W. Koshibae, N. Nagaosa, Y. Tokura, and M. Kawasaki, Interface-driven topological Hall effect in $SrRuO_3-SrIrO_3$ bilayer, Sci. Adv. **2**, e1600304.

[102] X. Chen, J. Zhang, B. Liu, F. Hu, B. Shen, and J. Sun, Tuning magnetic anisotropy and Dzyaloshinskii-Moriya interaction via interface engineering in nonisostructural $SrCuO_2/SrRuO_3$ heterostructures, Phys. Rev. B **105**, 214428 (2022).

[103] N. Gao, S. G. Je, M. Y. Im, J. W. Choi, M. Yang, Q. Li, T. Y. Wang, S. Lee, H. S. Han, K. S. Lee *et al.*, Creation and annihilation of topological meron pairs in in-plane magnetized films, Nat. Commun. **10**, 5603 (2019).

[104] H. Z. Wu, B. F. Miao, L. Sun, D. Wu, and H. F. Ding, Hybrid magnetic skyrmion, Phys. Rev. B **95**, 174416 (2017).

[105] S. Jiang, S. Liu, Y. Wang, W. Chen, H. Yin, B. Wang, C. Liu, Z. Feng, and G.-P. Zheng, Ferroelectricity in novel one-dimensional $P4_2$-InSeI nanowires, Results Phys. **31**, 104960 (2021).

[106] X. Lu, R. Fei, L. Zhu, and L. Yang, Meron-like topological spin defects in monolayer $CrCl_3$, Nat. Commun. **11**, 4724 (2020).